Soft Matter

Combined electrokinetic and shear flows control colloidal particle distribution across microchannel cross-sections

Journal:	*Soft Matter*
Manuscript ID	SM-ART-09-2020-001646.R1
Article Type:	Paper
Date Submitted by the Author:	28-Oct-2020
Complete List of Authors:	Lochab, Varun; The Ohio State University, Department of Mechanical and Aerospace Engineering Prakash, Shaurya; The Ohio State University, Department of Mechanical Engineering

Soft Matter

PAPER

Combined electrokinetic and shear flows control colloidal particle distribution across microchannel cross-sections

Varun Lochab[a], and Shaurya Prakash[a*]

Recent experimental observations on combined electrokinetic and shear flows of colloidal suspensions in rectangular cross-section microfluidic channels have shown unusual cross-stream colloidal particle migration and dynamic assembly. Although a new electrophoresis-induced lift force has been postulated to cause the lateral migration of colloidal particles, little is known about how fluid properties and flow conditions impact this force and therefore subsequent colloidal particle migration. Furthermore, no experimental quantification of this electrophoresis-induced lift force is available. We report several key advances by demonstrating that the kinematic viscosity of the fluid can be used to modulate the spatial distribution of particles over the entire microchannel cross-section, with suppression of the colloidal particle migration observed with increase in fluid kinematic viscosity. Colloidal particle migration of ~10 µm from not only the top and bottom microchannel walls but also from the side walls is shown with the corresponding electrophoresis-induced lift force of up to ~30 fN. The breadth of flow conditions tested capture the channel Reynolds number in the 0.1 – 1.1 range, with inertial migration of colloidal particles shown in flow regimes where the migration was previously thought to be ineffective, if not for the electrophoresis-induced lift force. The ability of the electrophoresis-induced lift force to migrate colloidal particles across the entire microchannel cross-section establishes a new paradigm for three-dimensional control of colloidal particles within confined microchannels.

1. Introduction

Accurately controlling the spatial distribution of microscale and nanoscale particles within a fluid flow can facilitate new applications in particle trapping[1, 2], separating[3], and sorting[4-6] for lab-on-a-chip systems[4, 7]. Further, emerging applications utilizing the promise of nanomaterials require unique particle assembly techniques[8-14] to fabricate structures with tunable functional properties at high throughput[15, 16]. This wide array of applications has enabled related theoretical and computational efforts[17-19] to understand fluid-particle interactions while evaluating the role of engineering the fluid flows[20, 21], especially in microfluidic channels.

Fluid flows in microfluidic channels traditionally operate in the low Reynolds number (Re, which is the ratio of inertial forces to viscous forces) regime, i.e., viscous forces dominate fluid inertia. Therefore, the effect of fluid inertia is typically neglected in these microscale flows. However, the underlying assumption for lack of inertial effects in microscale flows was challenged in the last decade, with demonstrations of unusual particle dynamics, including cross-stream (or perpendicular to the direction of fluid flow) particle migration[20, 22]. These demonstrations showed that, under specific conditions, non-negligible fluid inertia could be used for manipulating microscale particles (typical particle diameter > 1 µm) leading to the development of 'inertial microfluidics'[7, 22]. The basic premise of inertial microfluidics is that in fluid flow with finite inertia the particle positions within a microchannel can be manipulated by hydrodynamic inertial lift forces. These inertial lift forces were expected to vanish when the confinement ratio, defined as the ratio of particle radius (a) to the microchannel height (H), $a/H \ll 1$. Consequently, most reports for inertial migration and related applications in microfluidics are limited to particle diameters ~1-10 µm with microchannel critical dimensions ~O(100 µm). Moreover, it was generally believed that for smaller colloidal particles ($2a$ ~ 0.1-1 µm), manipulating particle position in microchannels by using fluid inertial forces would be ineffective.

However, Cevheri and Yoda[23] reported abnormal colloidal particle dynamics for particle radii ~ 0.25 µm in microchannels with H ~ 35 µm (i.e., a/H ~ 0.007 or $a/H \ll 1$). They showed near-wall (within ~ 0.5 µm of the channel wall) particle crowding and formation of distinct particle bands in combined electrokinetic and shear (specifically, Poiseuille) flows for a variety of applied electric fields and shear rates[23, 24]. Recently, we demonstrated novel colloidal particle dynamics in the channel *bulk* for these combined flows, i.e., when the particle distance from the microchannel walls (d) >> characteristic Debye length (λ_D) at channel walls in rectangular glass-poly(dimethylsiloxane) or glass-PDMS microchannels. We reported the colloidal particle dynamics as a function of particle size, particle zeta-potentials ζ_p, and background electrolyte concentration for a limited set of flow conditions[20]. The bulk migration of colloidal particles was shown to occur for particle radius down to 0.1 µm and a/H ~ 0.003. Specifically, we showed that the electrophoretic particle

[a] Department of Mechanical and Aerospace Engineering, The Ohio State University, Columbus, OH 43210, USA. *E-mail: prakash.31@osu.edu

†Electronic Supplementary Information (ESI) available: ESI is attached.

slip or the difference between the particle velocity and the background fluid velocity causes colloidal particles to migrate laterally with respect to the background fluid (electrolyte) flow along the microchannel length[20]. The colloidal particles concentrated towards the middle (bulk) of the microchannel cross-section when particles lagged the fluid flow, i.e., particle velocity < fluid velocity but the particles migrated towards the microchannel walls before particle assembly into band structures when colloidal particle velocity was higher than the fluid velocity. These findings, along with emerging theoretical models[18, 19] suggested that the unexpected fluid inertia-driven colloidal particle migration may occur due to a new electrophoresis-induced inertial lift force, which appears to be qualitatively similar to the broadly defined slip-shear effects[23, 25, 26]. Notably, near-wall colloidal particles ($d \sim O(a)$) could also experience Maxwell-stress induced electrical or dielectrophoretic-like lift forces[27-32] proportional to E_∞^2, where E_∞ is the externally applied electric field. However, such a functional dependence for the lift force on the electric field results in a repulsive lift-force; whereas in combined electrokinetic and Poiseuille flows, previous reports[20, 23, 24] have shown that the direction of particle migration and therefore presumably the direction of the lift force can be either repulsive or attractive with a first order dependence on the electric field[33], i.e., proportional to E_∞. Furthermore, it has been noted that electrokinetic or electroviscous lift forces[34-39] vanish for particle migration in channel bulk for the thin electric double layer limit[19]. Notably, the results reported here show particle migration on the order of several μm away from the microchannel walls in the thin electric double layer limit. Such unusual migration of colloidal particles in the channel bulk for combined flows was only recently addressed partially by theoretical models of electrophoresis-induced inertial lift force[18, 19]. It should also be noted that the electrophoresis-induced particle (diameter > μm) migration has been recently demonstrated and analyzed for viscoelastic shear flows[40-42]. The particle migration in viscoelastic flows was enhanced by interacting electrokinetic and rheological effects at dilute polymer concentrations[42]; however, at higher polymer concentrations particle migration opposite to that seen in Newtonian fluids was observed[40].

Despite the vast body of literature for particle migration in shear flows[17, 43-50], emerging results in inertial microfluidics[7, 22], and the newly identified electrophoresis-induced lift force[19, 20, 24] for colloidal particle migration in these combined (electrokinetic and shear) flows, a detailed evaluation and quantification for electrophoretic-slip induced lift is absent. We hypothesized that engineered flow through the manipulation of fluid properties and operational flow parameters (e.g., electric potential and pressure gradients) could be used to change spatial distributions of colloidal particles within the entire microchannel cross-section systematically. Consequently, in this paper, we present a broad and systematic quantification of colloidal particle migration in the microchannel bulk due to electrophoresis-induced lift forces. In a significant new finding, we report the first evidence of the effect of changing fluid density and viscosity on the particle migration and demonstrate that the migration due to fluid inertial effects can be suppressed as the fluid viscosity increased. Furthermore, we quantify the extent of particle migration, including that from side walls for controlling particle distributions in the entire cross-section of the microchannel as a function of easily accessible flow parameters.

2. Experimental methods

2.1 Device fabrication and particle migration imaging

The schematic for device operation and confocal microscopy imaging is shown in Figure 1. All experiments were performed using hybrid glass-poly(dimethylsiloxane) (PDMS) microfluidic channels with fabrication procedures reported previously[20]. Briefly, PDMS microchannels with dimensions 4 cm [L] × 340 μm [W] × 34.6 μm [H] were cast over a silanized SU-8 (PR; SU-8 2025, MicroChem Corp., Newton, MA) mold[20, 51] supported on a silicon wafer. Inlet and outlet for microchannels were punched using 3 mm biopsy punch (Integra Miltex) and the final microfluidic devices were obtained by bonding a borosilicate cover glass (Corning cover glass, #1.5) over the PDMS microchannels using O_2 plasma at 45 W RF power and 280 mTorr pressure for an exposure time of 40 s[20].

A 0.33% (w/w) colloidal suspension of carboxylate-functionalized particles with radius a = 240.0 ± 5.5 nm (Lot Number: 2016943, F8813, Thermo Fisher Scientific) was prepared in deionized water (18.2 MΩ·cm at 25°C) with sodium tetraborate decahydrate salt, $Na_2B_4O_7{\cdot}10H_2O$ (GFS Chemicals, ACS Grade) at a representative concentration of 1 mM as background electrolyte. Fluid viscosity was modified by adding glycerol (Sigma-Aldrich, ACS grade) to the electrolyte solution with $\{0, 10, 20, 30\}$ % (w/w) glycerol used. The fluid kinematic viscosity almost doubles in the 0-30 % (w/w) glycerol range for the Newtonian water-glycerol mixture[52, 53]. The colloidal particles were neutrally buoyant throughout the conditions tested. The concentration of electrolyte was kept constant at 1 mM in all the buffer solutions while the ζ_P for F8813 carboxylate-functionalized particles was -44.00 ± 9.00 mV as reported previously[20, 24].

The electrical connections across the microchannel were provided using stainless steel electrodes (diameter ~ 0.6 mm) inserted in the microchannel reservoirs with the pressure difference for the shear (Poiseuille) flow in the microchannels applied using a volumetric flow rate-controlled programmable syringe pump (PicoPlus, Harvard Apparatus) (14). An average electric potential gradient ($|\Delta V_{12}/L|$ in the range: 0 – 100 V/cm) was applied with the shear flow governed by volumetric flow rate in the 1 to 12 μL/min range. Both the electric potential gradient and the pressure gradient for Poiseuille flow were applied in the same direction.

Confocal imaging has been recently used to illuminate particle dynamics in both shear and electrokinetic flows[20, 54]. An Olympus spectral inverted FV3000 confocal imaging microscope with a resonant scanner and automatic stage control was utilized for imaging of the spatial distribution of colloidal particles within the microchannel (Figure 1a). The scanning speed of the resonant scanner was 66 ms per frame while the frame size chosen for confocal imaging through a 40x immersion oil objective was 512 pixels (318.20 μm; x) × 512 pixels (318.20 μm; y) as previously

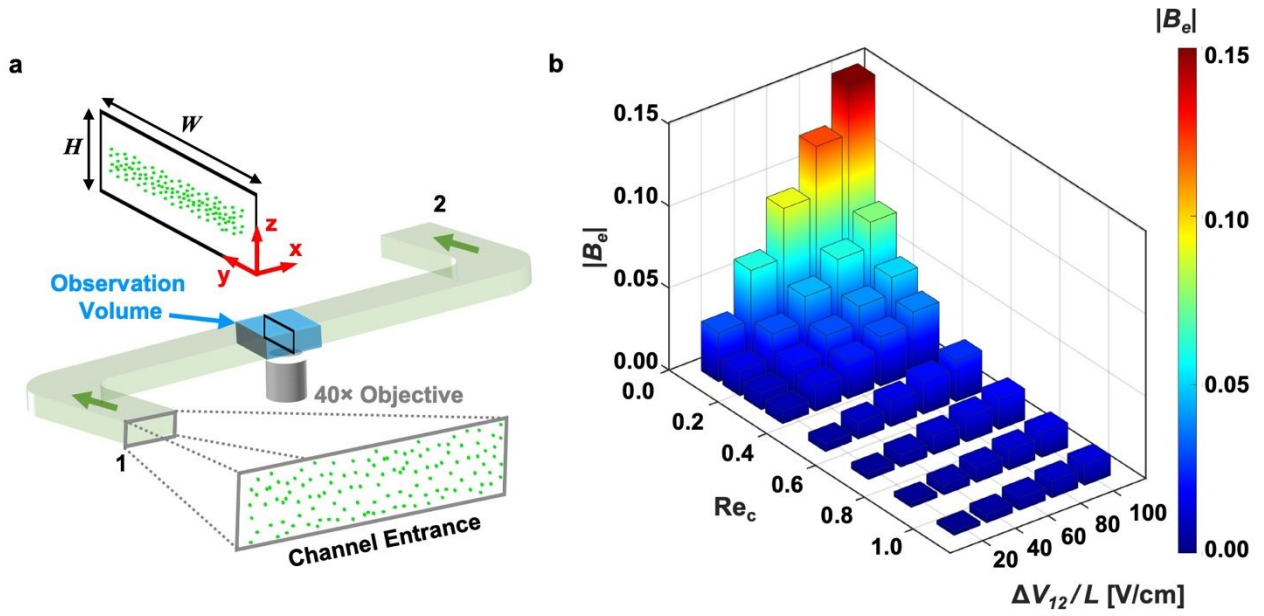

Figure 1. Microchannel schematic for confocal microscopy. (a) Schematic of a rectangular cross-section microchannel is shown where *H* and *W* are the height and width of the channel, respectively. The flow direction is shown in green arrows. The electric potential and pressure gradient were applied along the channel length between the channel inlet (1) and the channel outlet (2). Resonant scanner confocal imaging was used to observe the middle of the channel at 2 cm from the channel inlet, where the observation volume is shown as a blue box and a cross-section schematic is shown to demonstrate observed particle migration. (b) The magnitude of B_e is shown as a function of channel Reynolds number Re_c and $\Delta V_{12}/L$; $|B_e|$ decreases with increasing Re_c or decreasing electric field.

reported[20]. The numerical aperture (NA) for the objective (Olympus UPlanFLN 40x oil) was 1.30, refractive index (n) of oil was 1.518, and depth of focus ~ 0.956 µm. *Z*-stack imaging[20] (slice thickness = 1 µm) was used for visualizing colloidal particles across the channel depth in a volume scan with the particle fluorescence in green with respect to the dark (black) background reported in all the images. The spatial distribution of colloidal particles was observed at ~2 cm (fixed window) from channel inlet (Fig. 1a), as previously reported[20]. No individual particle tracking was performed in this report. The reported quantification arises from an average of three distinct measurements for each flow condition within microchannel devices (Figure 1).

The extent of the colloidal particle migration from the top and bottom walls (in the *z*-direction) was estimated by the width of the depletion zone near the channel walls as reported previously[20]. Specifically, Gaussian fits for intensity profiles across the channel height (*cf.* Figure 1a) were used to estimate the average extent of migration from the top and bottom walls (or the width of the depletion zone, d_z)[20]. Since a refractive index matched fluid[54, 55] was not used in this report, only average extent of depletion zone from top and bottom walls is reported. Using this past methodology for d_z, the extent of the depletion zone from the side walls d_y was estimated. All error bars represent the root-mean-square (rms) variance from the mean of three distinct measurements.

2.2 Experimental estimation of the electrophoresis-induced lift force

Past work with larger particles (diameter > 1 µm) has reported that at steady-state the particles establish an equilibrium position within the microchannel[7, 43, 46, 56]. Moreover, at these equilibria positions for non-accelerating particles hydrodynamic drag balances the electrophoresis-induced lift force[18]. By using the existing theoretical framework[18, 19], the corresponding electrophoresis-induced lift (EIL) force components in *y* and *z* were estimated as $EIL_y = 6\pi\mu a v_{m,y}$ and $EIL_z = 6\pi\mu a v_{m,z}$, where the average migration velocities $v_{m,y}$ and $v_{m,z}$ in *y* and *z*, respectively, were estimated from the ratio of depletion zones (d_z, d_y) and the time taken for particle distributions to reach steady-state at ~2 cm from inlet, where all observations were recorded, as reported previously[20, 24]. The time required to estimate the velocity from the measured depletion zone was determined during steady state operation (see Fig. 1a), i.e., when a time-invariant depletion region was observed to have been established with particles away from the microchannel walls. Therefore, the time needed for cross-stream particle migration is the time elapsed for particles to translate ~2 cm under steady state conditions from the channel inlet[20].

2.3 Flow description and relevant non-dimensional groups

Figure 1a shows the schematic for the experimental set-up comprising the microfluidic device and characterization of the colloidal migration using confocal microscopy under combined electrokinetic and shear flows[20]. The fluid-particle interactions in such flows are governed by several distinct phenomenological length and velocity scales. The microchannel aspect ratio defined as microchannel height to microchannel width (H/W) was ~ 0.1. A fixed background electrolyte concentration at pH 9 was used for all experiments (Debye length λ_D ~ 7 nm) as reported previously[20]. The reported pKa of glycerol is 14.4[57], and therefore it is not expected to dissociate appreciably and change the ionic composition of the buffer. Notably, $\lambda_D << a$ (0.24 µm), *H* (34.6 µm), and *W* (340 µm). The

results reported here are obtained for the thin electric double layer limit, i.e., λ_D/a << 1. Therefore, following the existing theoretical framework[18, 19], double layer relaxation effects and effects of streaming potentials were not considered. Moreover, the lift force corresponding to screening cloud distortions caused by particle translation and rotation have been reported; however, the theoretical estimate of the magnitude of the lift force was found to be ~6 orders of magnitude lower than the experimental observations[58].

The electrophoretic number (B_e) was defined as the ratio of the electrophoretic velocity of the colloidal particle introduced by the application of the electric field and the maximum fluid velocity ($\bar{u}_m$) due to the background Poiseuille flow[20]. Therefore, B_e uniquely labels the state of a colloidal particle moving through shear flow with different electric fields and flow rates. The trends in B_e as a function of experimentally evaluated flow conditions are shown in Figure 1b. The Reynolds number based on H was defined as $\mathrm{Re_c} = \rho\bar{u}_m H/\mu$, where ρ and μ are fluid density and dynamic viscosity, respectively, and $\mathrm{Re_c}$ represents the ratio of inertial to viscous forces for the characteristic length H. At a given flow rate Q, i.e., for a fixed $\mathrm{Re_c}$, B_e increases (Figure 1b) with the average electric field ($\Delta V_{12}/L$) due to the increase in the particle electrophoretic velocity.

For colloidal particle migration, a Reynolds number with the particle radius as the characteristic length scale is also an important parameter as defined earlier[19, 48]. For a particle radius a, $\mathrm{Re_p} = \rho\bar{u}_m\alpha a/\mu = \alpha^2\mathrm{Re_c}$, where $\alpha = a/H$[19, 48]. The results reported here are for $0.1 \le \mathrm{Re_c} \le 1.1$ mapping the fluid flow regimes from weakly inertial flows ($\mathrm{Re_c}$ << 1) to $\mathrm{Re_c}$ ~ 1 flows with finite fluid inertia[18, 19, 48]. Consequently, $\mathrm{Re_p} = \mathrm{Re_c}\,\alpha^2$ ranges from 4.2×10^{-6} to 5.1×10^{-5} or $\mathrm{Re_p}$ << 1 for all experiments.

3. Results and discussion

3.1 Effect of fluid viscosity on inertial migration of colloidal particles

Prevailing knowledge[18-20] suggests that fluid inertia is essential to lateral or cross-stream colloidal particle migration. Yet, no explicit experimental investigation of particle migration on changing the fluid properties that affect the relative contribution of inertial and viscous

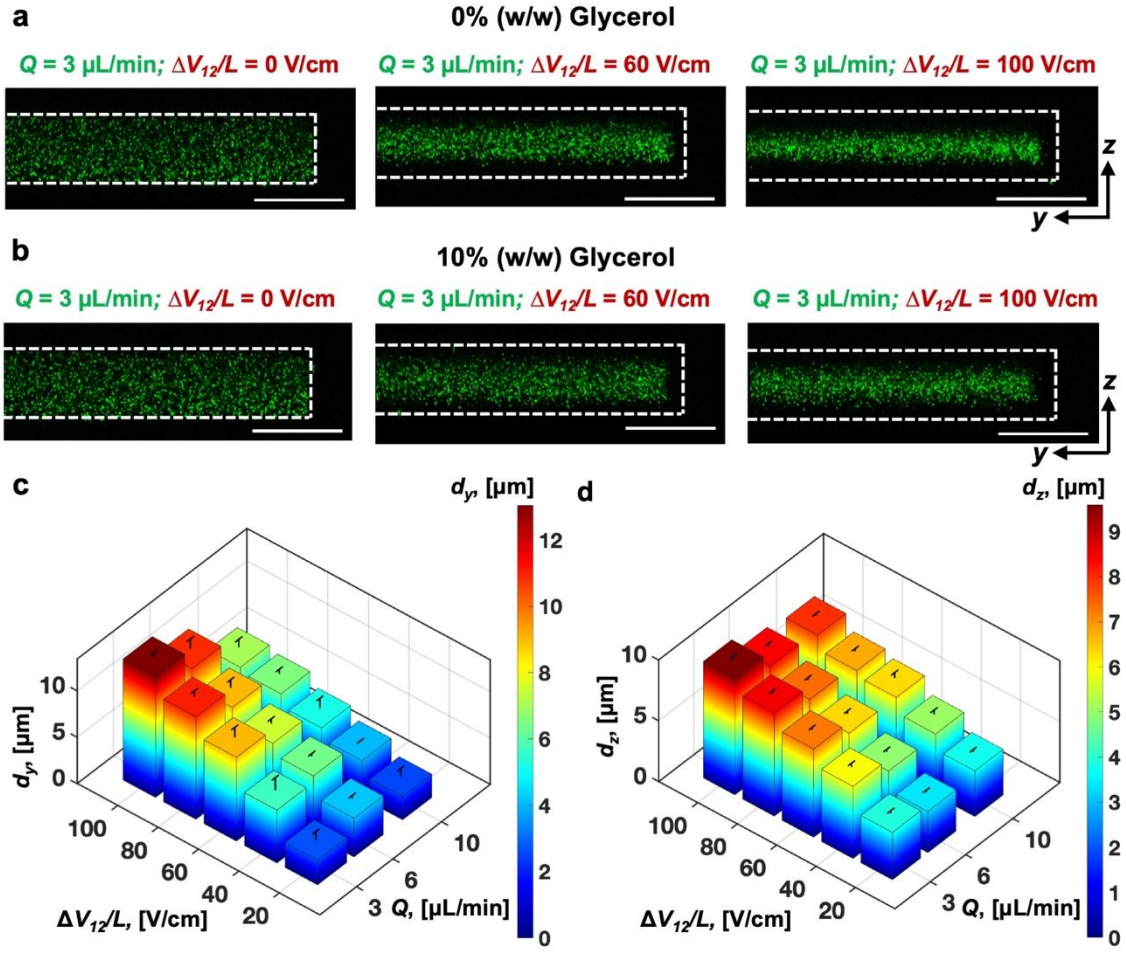

Figure 2. Effect of changing fluid kinematic viscosity. Comparison of cross-section views from the observation area (*cf.* Figure 1a), where the flow is going into the page for (a) 0% (w/w) glycerol, (b) 10% (w/w) glycerol. Cross-section views are from half of the channel width (*cf.* Figure 1a). The scale bar is 50.00 μm. Quantitative estimates for both d_y and d_z as a function of Q and $\Delta V_{12}/L$ for 10% (w/w) glycerol are shown in (c) and (d), respectively. Error bars represent rms variance from the mean for three different measurements for each tested flow condition.

forces have been reported to evaluate this postulation. Therefore, the properties of the aqueous buffer used for preparing colloidal suspension were adjusted with glycerol at {0, 10, 20, 30}% (w/w), where the fluid kinematic viscosity increased with increasing glycerol weight fraction (Supplementary Information, Figure S1) and more than doubles over the selected range. As the glycerol fraction was increased, the viscous forces increased compared to the fluid inertial forces. It should be noted that the change in density of the buffer solution, however, was 1 g/cm^3 at 0 % (w/w) to ~1.07 g/cm^3 at 30 % (w/w). In comparison, the colloidal particles, were 1.05 g/cm^3, and therefore, considered nearly neutrally buoyant[20], with negligible force due to gravity (approximately 10^{-27} N).

Figures 2a and 2b show that the colloidal particles migrated towards the centre of the channel in agreement with past results for the aqueous buffer with no added glycerol (0% (w/w))[20]. Only half the channel cross-section is shown due to channel symmetry (Figure 1a). The extent of particle migration (Figure 2a) increased at a given flow rate as the strength of the applied electric field was increased, with a corresponding increase in B_e (Figure 1b). At 10% (w/w) glycerol, the kinematic viscosity (Supplementary Information, Figure S1) increased by ~25% compared to the 0% (w/w) glycerol buffer. The migration of colloidal particles towards the microchannel centre was suppressed compared to that observed at 0% (w/w) glycerol leading to a visually observed broader spatial distribution of particles (Figures 2a-2b).

Figures 2c and 2d show the estimated colloidal particle migration in both directions, i.e., d_y (from the side walls towards channel centre; along the y-direction) and d_z (migration from the top or bottom wall towards channel centre; along the z-direction) for 10% (w/w) glycerol. Quantitatively, the extent of particle migration in the y-direction increased as the electric field was increased at 10% (w/w) glycerol (Figure 2c) for a given flow rate. For example, at 3 µL/min ($Re_c \approx 0.21$), d_y was 2.67 $\pm$ 0.92 µm and 13.04 $\pm$ 0.41 µm at $\Delta V_{12}/L$ = 20 V/cm ($|B_e|$ = 0.008) and $\Delta V_{12}/L$ = 100 V/cm ($|B_e|$= 0.0392), respectively; similarly, at 10 µL/min ($Re_c \approx 0.70$), d_y was 2.51 $\pm$ 0.87 µm at $\Delta V_{12}/L$ = 20 V/cm ($|B_e|$ = 0.002) and 7.02 $\pm$ 0.87 µm at $\Delta V_{12}/L$ = 100 V/cm and $|B_e|$ = 0.012 (Figure 2c). Once again, with increasing electric field strength five-fold, B_e also increases proportionally, while the observed extent of colloidal particle migration increased by ~5 times at 3 µL/min ($Re_c \approx 0.21$) and ~2.8 times at 10 µL/min ($Re_c \approx$

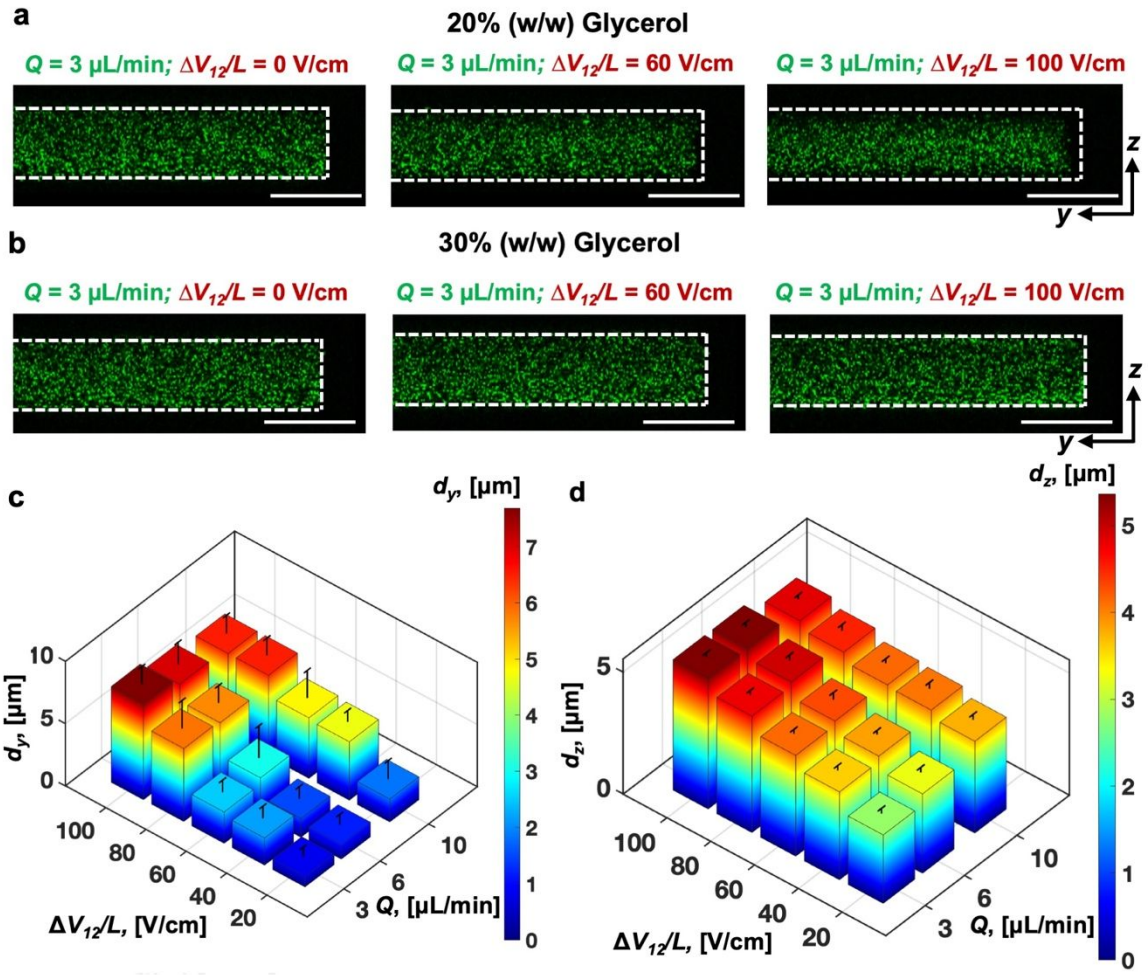

Figure 3. Effect of changing fluid kinematic viscosity. Comparison of cross-section views from the observation area (cf. Figure 1a), where the flow is going into the page for (a) 20% (w/w) glycerol, (b) 30% (w/w) glycerol. Cross-section views are from half of the channel width (cf. Figure 1a). The scale bar is 50.00 µm. Quantitative estimates for both d_y and d_z as a function of Q and $\Delta V_{12}/L$ for 20% (w/w) glycerol are shown in (c) and (d), respectively. Notably, at 30% (w/w) glycerol particle migration was within the spatial resolution limit of the confocal microscope demonstrating a substantially lower (< 2 µm) extent of migration from the microchannel walls compared to the 0% (w/w) glycerol case. Error bars represent rms variance from the mean for three different measurements for each tested flow condition.

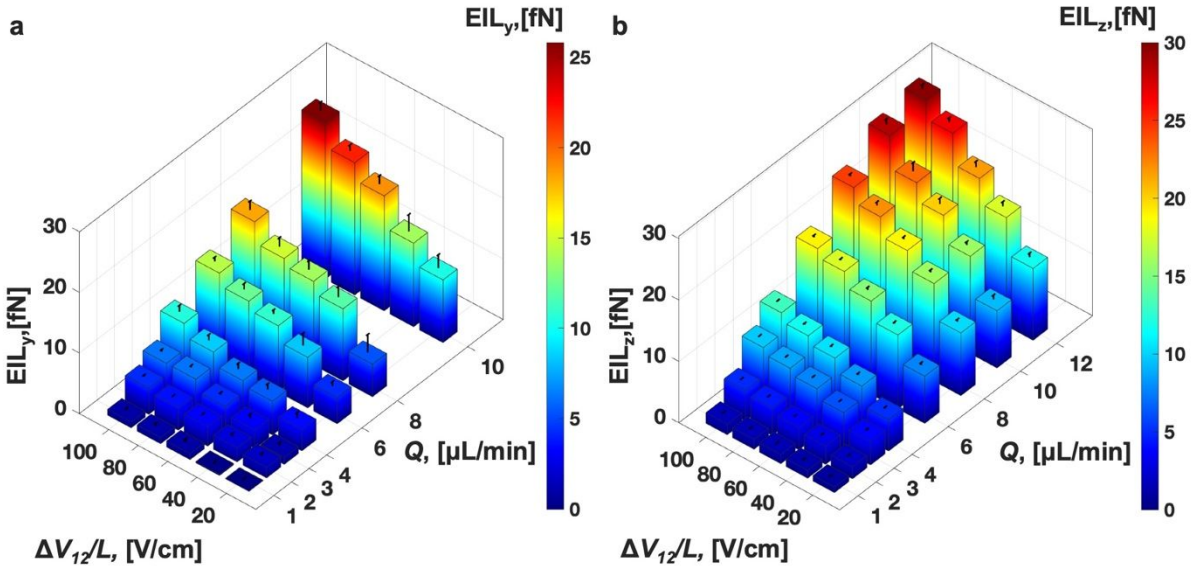

Figure 4. Experimental estimates of electrophoresis induced lift (EIL, fN) force. (a) In *y*-direction EIL_y and (b) in *z*-direction EIL_z are seen. EIL_y and EIL_z both increase as a function of flow rate and the average electric field with maximum experimentally estimated lift force of ~ 30 fN. All data reported in this figure was obtained at 0 % (w/w) glycerol with overall trends remaining similar for the remaining glycerol weight fractions added to the aqueous buffer. Error bars represent rms variance from the mean for three different measurements for each tested flow condition.

0.70). Figure S2 (Supplementary Information) shows changes in B_e as a function of flow conditions at 10% (w/w) glycerol. In comparison, keeping the average electric field fixed, for example at $\Delta V_{12}/L$ = 60 V/cm, it was noted that d_y decreased from 9.03 ± 1.08 μm at Q = 3 μL/min ($Re_c \approx 0.21$) to 5.18 ± 1.04 μm at Q = 10 μL/min ($Re_c \approx 0.70$).

Similarly, for particle migration in the *z*-direction, the extent of migration increased with an increasing electric field (Figure 2d) for a given volumetric flow rate. For example, at Q = 3 μL/min ($Re_c \approx 0.21$), d_z was 3.89 ± 0.21 μm and 9.59 ± 0.22 μm at $\Delta V_{12}/L$ = 20 V/cm ($|B_e|$ = 0.008) and $\Delta V_{12}/L$ = 100 V/cm ($|B_e|$ = 0.0392), respectively; whereas at Q = 10 μL/min ($Re_c \approx 0.70$), d_z was 3.75 ± 0.18 μm at $\Delta V_{12}/L$ = 20 V/cm ($|B_e|$ = 0.002) and 7.96 ± 0.17 μm at $\Delta V_{12}/L$ = 100 V/cm and $|B_e|$ = 0.012. Similar to the trends for d_y, d_z also decreased with an increased flow rate (or Reynolds number, Re_c) at a fixed electric field. For example, at an average electric field $\Delta V_{12}/L$ = 60 V/cm, d_z decreased from 7.26 ± 0.19 μm at Q = 3 μL/min ($Re_c \approx 0.21$) to 6.32 ± 0.46 μm at Q = 10 μL/min ($Re_c \approx 0.70$). The complete data sets for the three flow rates and five electric fields are reported in Figure S3, Supplementary Information, with overall trends remaining similar to Figures 2c and 2d. Notably, by manipulating the respective electrokinetic and shear flow conditions, the extent of colloidal migration can be controlled at a given fluid kinematic viscosity. It was observed that the maximum extent of colloidal particle migration was on the order of 10 μm both along *y*-direction and *z*-direction with the majority of the particles confined near the middle of the microchannel and away from all the enclosing microchannel walls.

Figures 3a and 3b show visually that the extent of particle migration in the *y* and *z*-directions continues to decrease as the kinematic viscosity was increased. For example, at 3 μL/min and 100 V/cm, the extent of migration from the channel side-wall d_y = 13.04 ± 0.41 μm at 10% (w/w) glycerol ($Re_c \approx 0.21$), but d_y = 7.69 ± 1.39 μm at 20% (w/w) glycerol ($Re_c \approx 0.16$), which is a 41% decrease in *y*-direction migration as compared to 10% (w/w) glycerol. Similarly, the extent of migration in the *z*-direction, i.e., along the depth of the channel also decreases as kinematic viscosity was increased; at 3 μL/min and 100 V/cm, d_z = 9.59 ± 0.22 μm at 10% (w/w) glycerol ($Re_c \approx 0.21$) but d_z = 5.36 ± 0.17 μm at 20% (w/w) glycerol ($Re_c \approx 0.16$). Note that, as the Re_c decreased by 23%, the extent of migration along *z* had decreased by 44 %.

At 30% (w/w) glycerol, the migration was suppressed to within ~ 2 μm of the microchannel walls in both the *y* and *z* directions and is within the spatially unresolved resolution of the confocal microscope (Figure 3b). Therefore, visually it appears that the spatial distribution of neutrally buoyant but charged dielectric particles can be manipulated to a nearly uniform distribution across the entire cross-section at high enough kinematic viscosity.

The kinematic viscosity more than doubled from 0.9×10^{-6} m^2s^{-1} to 2.0×10^{-6} m^2s^{-1} as glycerol fraction was increased from at 0% (w/w) to 30% (w/w). It can be surmised that the viscous forces increased by a factor of more than 2x compared to the inertial forces; however, the extent of particle migration did not change in the same proportion to the change in fluid properties with a visually uniform distribution observed at 30% (w/w) glycerol, suggesting a non-linear dependence of lift forces on the kinematic viscosity. Taken together, the results in Figure 2 and Figure 3 show for the first time that the colloidal particles can be concentrated away from the microchannel walls with the spatial distribution or the extent of the migration controlled by fluid viscosity and the flow conditions.

3.2 Experimental estimation of electrophoresis-induced lift force components.

To our knowledge, no reports have experimentally estimated the electrophoresis-induced lift (EIL) force experienced by colloidal particles which control the dynamics of cross-stream particle migration (Figure S4) in the microchannel bulk under combined electrokinetic and shear flows. The corresponding EIL force components in the *y* and *z*-direction are shown in Figures 4a and 4b respectively. EIL force components in both directions for an extensive set of flow conditions was noted to increase monotonically as a function of both flow rate (and therefore, Re_c) and applied electric field (and therefore, B_e).

For example, along the *y*-direction, for a given flow rate of Q = 3 µL/min ($Re_c \approx 0.26$), EIL_y increases from 1.15 ± 0.50 fN at $\Delta V_{12}/L$ = 20 V/cm ($|B_e| = 0.010$) to EIL_y = 6.17 ± 0.35 fN at $\Delta V_{12}/L$ = 100 V/cm ($|B_e| = 0.050$). On the other hand, for a constant $\Delta V_{12}/L$ = 100 V/cm, EIL_y was 0.96 ± 0.39 fN at Q = 1 µL/min ($Re_c \approx 0.09$) but it increases to 25.82 ± 1.41 fN at Q = 12 µL/min ($Re_c \approx 1.05$). Similarly, along the *z*-direction, for Q = 3 µL/min, EIL_z increased from 3.80 ± 0.19 fN at $\Delta V_{12}/L$ = 20 V/cm ($|B_e| = 0.010$) to EIL_z = 9.68 ± 0.15 fN at $\Delta V_{12}/L$ = 100 V/cm ($|B_e| = 0.050$). Furthermore, at a constant applied electric field of $\Delta V_{12}/L$ = 100 V/cm, EIL_z was 1.71 ± 0.12 fN at Q = 1 µL/min ($Re_c \approx 0.09$) but increases to EIL_z = 29.69 ± 0.69 fN at Q = 12 µL/min ($Re_c \approx 1.05$). The corresponding migration velocities along *y* and *z* are provided in Figure S5, S6 in Supplementary Information.

It is worth noting that the two recently published theoretical models[18, 19] qualitatively capture the direction of the EIL force; however, the estimated magnitudes are dramatically under-predicted. Both these models are limited to weakly inertial flows ($Re_c << 1$ or $Re_p << \alpha^2$) or for small but non-negligible fluid inertia but predict electrophoresis-induced lift force due to particle slip on the same order of magnitude as $O(B_e Re_p)$, which increases as the electric field (through electrophoretic number) and flow rate (through Reynolds number) is increased. Moreover, the models are limited to flow between parallel infinite planes as opposed to a rectangular-slit glass-PDMS channels used in experiments. In a significant departure, existing models do not predict lift force components from the side walls of the microchannel.

Using the model by Khair *et al.*[18] for the experimental parameters reported here, EIL_z was estimated to be ~10^{-17} N, or 10^{-2} fN for the Q = 12 µL/min and $\Delta V_{12}/L$ = 100 V/cm, and ~10^{-3} fN for Q = 1 µL/min and $\Delta V_{12}/L$ = 100 V/cm. By contrast, the experimental lift force component along *z* were 3 orders of magnitude larger, EIL_z = 29.69 ± 0.69 fN for Q = 12 µL/min and $\Delta V_{12}/L$ = 100 V/cm (Figure 4b) and 1.71 ± 0.12 fN for Q = 1 µL/min and $\Delta V_{12}/L$ = 100 V/cm.

The discrepancies between the experimental and theoretical results for electrophoresis-induced lift are not well understood. We postulate, for the results reported here that as $0.1 \le Re_c \le 1.1$, the experimental conditions are not limited to the weakly inertial flows considered for the theoretical models. Furthermore, for particle migration in a shear flow as opposed to an unbounded quiescent fluid, Saffman length is known to scale as $l_S \sim a/\sqrt{Re_p} \sim H/\sqrt{Re_c}$[59, 60]. l_S is the distance from the particle centre to a point in the fluid where inertial forces balance the viscous forces. Calculating l_S for the experimental data reported here for $0.1 \le Re_c \le 1.1$ yields $l_S \sim 3H$ for Re_c = 0.1 and $l_S \sim H$ for Re_c = 1.1.

In particular, if $l_S >> H$ for weakly inertial flows ($Re_c << 1$ or $Re_p << \alpha^2$) then the flow is considered to be well-bounded with viscous effects dominating, and the flow field is controlled by the boundary conditions at walls[60]. Consequently, the problem of a particle migrating in the fluid flow for $l_S >> H$ is a regular perturbation problem[60, 61]. However, when the channel dimensions are comparable to or greater than l_S (as is the case here) the flow around the particle should be split into two regions - a domain close to the particle representing the inner flow region and a far-field representing the outer flow region[48]. Such a problem was solved by Hogg[48] for the migration of non-neutrally buoyant particles but in the shear-flow only for $Re_c \sim 1$ using the method of matched asymptotic expansions[48]. To our knowledge, no such analysis or model exists for the present problem of combined electrokinetic and shear flows for neutrally buoyant particles. Moreover, it has been established that the flow around a particle undergoing electrophoresis is characteristically different from that of a non-neutrally buoyant particle under gravity[62, 63]. Clearly, further work is needed for theoretical models to validate against observed experimental results. As theoretical understanding and models continue to develop, considerations for hydrodynamic interactions between particles will likely need to be included as well. Lastly, colloidal particle diffusion dynamics is a function of confinement, particle position from the channel walls, and the flow conditions[64, 65]. Nonetheless, the Peclet number ($\bar{u}_m H/D_\infty$) based on channel centerline velocity at lowest flow rate (1 µL/min) and $D_\infty = k_B T/(6\pi\mu a)$ from Stokes-Einstein relation[65], where k_B is the Boltzmann constant and T is the room temperature, was of order 10^4. Therefore, the effects of diffusion on lateral particle migration in channel bulk could be neglected.

3.3 Quantification of colloidal particle migration in combined electrokinetic and Poiseuille flows

Figure 5a and Figure 5b report the quantified migration of colloidal particles from the side walls (d_y) and the top and bottom microchannel walls (d_z) for a broad range of flow conditions in order to map the particle dynamics in microchannels. Supplementary Information, Figure S4 shows confocal microscopy images showing that particle migration towards the microchannel centre was non-monotonic with respect to changing flow rate, where the particles moved the farthest at an intermediary flow rate, Q = 4 µL/min. For example, for a constant $\Delta V_{12}/L$ = 60 V/cm, d_z increased from 5.22 ± 0.23 µm at Q = 1 µL/min to 9.11 ± 0.22 µm at Q = 4 µL/min before decreasing back to 6.31 ± 0.28 µm at Q = 12 µL/min (Figure 5b). Similar trends in particle migration as function of flow rate were seen both along *y* and *z* at all other applied electric fields (Figure 5a, 5b).

In contrast, the migration of particles away from the walls typically increased monotonically with the applied average electric field at a given flow rate (Figure 5a, 5b). For example, at a fixed flow rate of Q = 4 µL/min, d_y increased from 3.01 ± 0.82 µm at $\Delta V_{12}/L$ = 20 V/cm to 9.19 ± 0.92 µm at $\Delta V_{12}/L$ = 100 V/cm. Similarly, for migration along the depth of the channel or along the *z*-direction, at Q = 4 µL/min, d_z increased monotonically from 4.46 ± 0.20 µm at $\Delta V_{12}/L$ = 20 V/cm to 11.44 ± 0.17 µm at $\Delta V_{12}/L$ = 100 V/cm.

Interestingly, even though both EIL_y and EIL_z increase monotonically with increased flow rate and electric field (Figure 4), the extent of migration shows a clear non-monotonic trend in migration as highlighted by the dotted pink square in Figure 5 for both d_y and d_z. Therefore, it appears that there is a competition between the migration laterally across the flow and the time taken for particles to reach their respective equilibrium positions. Notably, the time available for cross-stream particle migration decreases as the flow rate increases since particles travel faster to the region of observation from channel inlet (Figure 1a).

Surprisingly, not only do the particles (here, with a = 0.24 µm) show significant migration for $a/H << 1$, but this migration occurs on the same order from the side walls for the microchannel aspect ratio (H/W) of ~0.1. For example, the migration of colloidal particles from the side walls was found to be on the same order of magnitude as from the top and bottom walls; for example, d_y was ~9.19 ± 0.92 µm (Figure 5a) while d_z was ~11.44 ± 0.17 µm (Figure 5b) at 4 µL/min and

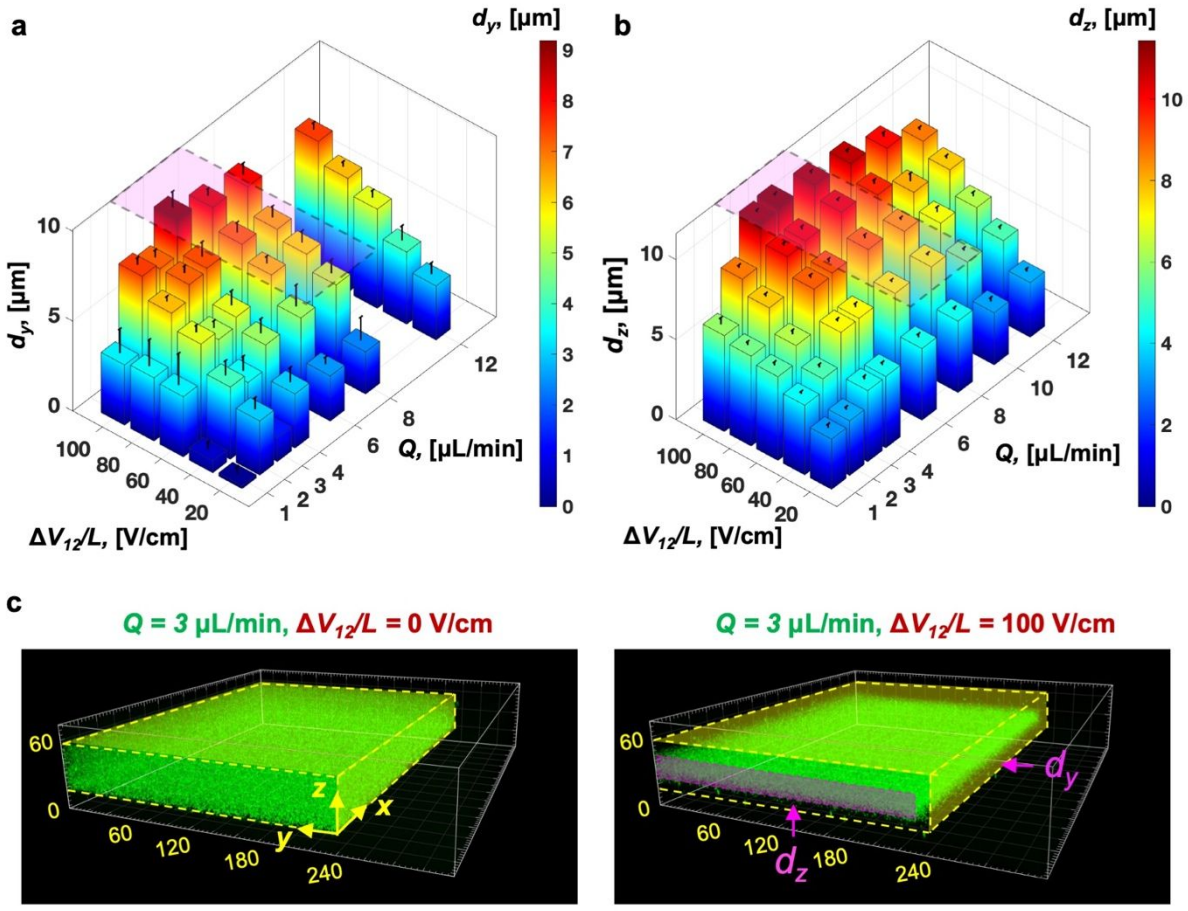

Figure 5. Quantification of colloidal particle migration. (a) d_y is along the *y*-direction and (b) d_z is along the *z*-direction. The extent of particle migration in both *y* and *z*-directions shows a non-monotonic behavior as a function of flow rate with the extent of migration observed to be the highest at intermediary flow rates (pink box) within the range of flow rates (1-12 µL/min) tested. Data reported in this figure was obtained at 0 % (w/w) glycerol but overall trends were similar at other kinematic viscosities. Error bars represent rms variance from the mean for three different measurements for each tested flow condition. (c) Visual representation of spatial particle distribution shows colloidal migration (pink box and arrows) at 3 µL/min from the top and bottom walls (marked as d_z), and one of the side-wall (marked as d_y) for two representative cases with the average electric field at 0 V/cm and 100 V/cm.

100 V/cm. The significance of the migration in the *y*-direction is that the average shear rate in the *y*-direction (normal to side-wall) is approximately one-tenth of the average shear rate in the *z*-direction (normal to the top and bottom walls), yet the extent of migration is comparable (Figure 5a, 5b). It is worth noting that quantifiable side-wall migration has not been reported previously and is also not captured by any of the existing models.

Colloidal particle migration in the *y*-direction suggests that the average shear stress controlled in experiments by the volumetric flow rate may not be the ideal parameter to evaluate colloidal particle migration. As a first-order estimate of the underlying flow physics, the well-known analytical flow profile due to only Poiseuille flow in the absence of particles is seen in the Supplementary Information, Figure S7a[66]. Interestingly, when the colloidal particle migration magnitude in *y* and *z* (i.e., d_y and d_z) were normalized with respect to the channel width and height, respectively, the magnitude of normalized local fluid shear rate was noted to be on the same order of magnitude at the normalized migration d_y/H and d_z/W (Supplementary Information, Figure S7b). These observations indicate that the electrophoretic lift force induced particle migration may possibly depend on local flow conditions rather than the average bulk flow parameters and requires further investigation, which is beyond the scope of the present work. Nevertheless, these observations show that the migration on the order of ~10 µm (or approximately 20 particle diameters) can be achieved in both the *y* and *z*-directions by engineering the flow conditions.

Finally, figure 5c shows a representative example for the well-mixed colloidal solution distributed uniformly through the microchannel cross-section. When the electric field was increased to 100 V/cm, as now expected, particle migration away from both the side walls and the top and bottom walls is seen, providing a visual example of the ability to control spatial distribution throughout the microchannel volume. Clearly, optimization of particle migration for specific applications will require further work as a function of not only flow conditions but also fluid properties and, possibly, the microchannel aspect ratio.

4. Conclusion

In this paper, the colloidal particle dynamics in Poiseuille flow with simultaneous applied electric fields was quantitatively characterized for a broad range of flow conditions and fluid properties with flow rates ranging from 1-12 μL/min, corresponding to the microchannel Reynolds number in the 0.1 to 1.1 range with strength of electric fields up to 100 V/cm.

First, the effect of changing fluid density and viscosity on the particle migration in combined electrokinetic and shear flows was shown for the first time. Specifically, the migration of colloidal particles showed a decrease as the kinematic viscosity was increased with increasing glycerol weight fraction in the solution, and the inertial effects were suppressed to a point where the migration was indiscernible at 30% (w/w) glycerol colloidal suspension to obtain a nearly uniform spatial distribution across the entire microchannel cross-section. The components of electrophoresis-induced lift force increased both as a function of flow rate and electric field strength. The lift force components were experimentally estimated to be in the range ~ 1 – 30 fN. The experimentally estimated lift force was significantly higher (~3 orders of magnitude) compared to existing theoretical models.

Quantification of particle migration showed that it is possible to control particle distributions across the entire microchannel cross-section by engineering microfluidic flows. With the results reported here, we present a potential method to achieve a high degree of control over colloidal particle positions within the flow field in microchannels while laying a basis for future theoretical development.

Conflicts of interest

There are no conflicts to declare.

Acknowledgements

The US Army Research Office funded this work through grant number W911NF-16-0278 and W911-NF-1-0144. Partial personnel support from the National Institutes of Health via award R01HL141941 is also acknowledged. We thank the Campus Microscopy and Imaging Facility, The Ohio State University. This facility is supported in part by grant P30 CA016058, National Cancer Institute, Bethesda, MD. We also thank the staff of Nanotech West for helping with device fabrication and characterization.

References

1. W. Liu, J. Shao, Y. Jia, Y. Tao, Y. Ding, H. Jiang and Y. Ren, *Soft Matter*, 2015, **11**, 8105-8112.
2. D. Vigolo, S. Radl and H. A. Stone, *Proceedings of the National Academy of Sciences*, 2014, **111**, 4770.
3. N. A. M. Yunus, H. Nili and N. G. Green, *Electrophoresis*, 2013, **34**, 969-978.
4. P. Sajeesh and A. K. Sen, *Microfluidics and Nanofluidics*, 2014, **17**, 1-52.
5. V. Velasco and S. J. Williams, *Journal of Colloid and Interface Science*, 2013, **394**, 598-603.
6. R. Johann and P. Renaud, *Electrophoresis*, 2004, **25**, 3720-3729.
7. J. Zhang, S. Yan, D. Yuan, G. Alici, N. T. Nguyen, M. Ebrahimi Warkiani and W. Li, *Lab on a Chip*, 2016, **16**, 10-34.
8. N. Vogel, M. Retsch, C. A. Fustin, A. Del Campo and U. Jonas, *Chemical Reviews*, 2015, **115**, 6265-6311.
9. V. N. Manoharan, *Science*, 2015, **349**, 1253751-1253758.
10. K. N. Plunkett, A. Mohraz, R. T. Haasch, J. A. Lewis and J. S. Moore, *Journal of the American Chemical Society*, 2005, **127**, 14574-14575.
11. Y. Xia, J. A. Rogers, K. E. Paul and G. M. Whitesides, *Chemical Reviews*, 1999, **99**, 1823-1848.
12. H. Tan, S. Wooh, H.-J. Butt, X. Zhang and D. Lohse, *Nature Communications*, 2019, **10**, 478.
13. M. Cavallaro, L. Botto, E. P. Lewandowski, M. Wang and K. J. Stebe, *Proceedings of the National Academy of Sciences*, 2011, **108**, 20923.
14. J. H. Park and N. R. Aluru, *Surface Science*, 2011, **605**, 1616-1620.
15. A. T. L. Tan, S. Nagelberg, E. Chang-Davidson, J. Tan, J. K. W. Yang, M. Kolle and A. J. Hart, *Small*, 2020, **16**, 1905519.
16. Z. Gong, T. Hueckel, G.-R. Yi and S. Sacanna, *Nature*, 2017, **550**, 234-238.
17. E. S. Asmolov, A. L. Dubov, T. V. Nizkaya, J. Harting and O. I. Vinogradova, *Journal of Fluid Mechanics*, 2018, **840**, 613-630.
18. A. S. Khair and J. K. Kabarowski, *Physical Review Fluids*, 2020, **5**, 033702.
19. A. Choudhary, T. Renganathan and S. Pushpavanam, *Journal of Fluid Mechanics*, 2019, **874**, 856-890.
20. V. Lochab, A. Yee, M. Yoda, A. T. Conlisk and S. Prakash, *Microfluidics and Nanofluidics*, 2019, **23**, 134.
21. P. Sundaram, L. Casadei, G. Lopez, D. Braggio, G. Balakirsky, R. Pollock and S. Prakash, *Journal of Microelectromechanical Systems*, 2020, **PP**, 1-7.
22. D. Di Carlo, *Lab on a chip*, 2009, **9**, 3038-3046.
23. N. Cevheri and M. Yoda, *Lab on a Chip*, 2014, **14**, 1391-1394.
24. A. Yee and M. Yoda, *Microfluidics and Nanofluidics*, 2018, **22**, 1-12.
25. H. Amini, W. Lee and D. Di Carlo, *Lab on a Chip*, 2014, **14**, 2739-2761.
26. Y. W. Kim and J. Y. Yoo, *Lab on a Chip*, 2009, **9**, 1043-1045.
27. E. Yariv, *Physics of Fluids*, 2006, **18**.
28. M. Yoda and Y. Kazoe, *Physics of Fluids*, 2011, **23**.
29. Y. Kazoe and M. Yoda, *Langmuir : the ACS Journal of Surfaces and Colloids*, 2011, **27**, 11481-11488.
30. L. Liang, Y. Ai, J. Zhu, S. Qian and X. Xuan, *Journal of Colloid and Interface Science*, 2010, **347**, 142-146.
31. L. Liang, S. Qian and X. Xuan, *Journal of Colloid and Interface Science*, 2010, **350**, 377-379.
32. E. Yariv, *Soft Matter*, 2016, **12**, 6277-6284.
33. N. Cevheri and M. Yoda, *Langmuir*, 2014, **30**, 13771-13780.
34. S. G. Bike and D. C. Prieve, *Journal of Colloid and Interface science*, 1995, **175**, 422-434.
35. S. G. Bike, L. Lazarro and D. C. Prieve, *Journal of Colloid and Interface Science*, 1995, **175**, 411-421.
36. O. Schnitzer, I. Frankel and E. Yariv, *Mathematical Modelling of Natural Phenomena*, 2012, **7**, 64-81.
37. O. Schnitzer, I. Frankel and E. Yariv, *Journal of Fluid Mechanics*, 2012, **704**, 109-136.
38. P. Warszyński, X. Wu and T. G. M. van de Ven, *Colloids and Surfaces A: Physicochemical and Engineering Aspects*, 1998, **140**, 183-198.
39. T. G. M. van de Ven, P. Warszynski and S. S. Dukhin, *Journal of Colloid and Interface Science*, 1993, **157**, 328-331.

40. D. Li and X. Xuan, *Physical Review Fluids*, 2018, **3**, 074202.
41. A. Zhang, W. L. Murch, J. Einarsson and E. S. G. Shaqfeh, *Journal of Non-Newtonian Fluid Mechanics*, 2020, **280**, 104279.
42. A. Choudhary, D. Li, T. Renganathan, X. Xuan and S. Pushpavanam, *Journal of Fluid Mechanics*, 2020, **898**, A20.
43. G. Segré and A. Silberberg, *Nature*, 1961, **189**, 209-210.
44. S. I. Rubinow and J. B. Keller, *Journal of Fluid Mechanics*, 1961, **11**, 447-459.
45. F. P. Bretherton, *Journal of Fluid Mechanics*, 1962, **14**, 284-304.
46. B. P. Ho and L. G. Leal, *Journal of Fluid Mechanics*, 1974, **65**, 365-400.
47. P. Vasseur and R. G. Cox, *Journal of Fluid Mechanics*, 1976, **78**, 385-413.
48. A. J. Hogg, *Journal of Fluid Mechanics*, 1994, **272**, 285-318.
49. E. S. Asmolov, *Journal of Fluid Mechanics*, 1999, **381**, 63-87.
50. F. Del Giudice, G. D'Avino, F. Greco, P. L. Maffettone and A. Q. Shen, *Physical Review Applied*, 2018, **10**, 064058.
51. D. C. Duffy, J. C. McDonald, O. J. A. Schueller and G. M. Whitesides, *Analytical chemistry*, 1998, **70**, 4974-4984.
52. K. Mann, S. Deutsch, J. Tarbell, D. Geselowitz, G. Rosenberg and W. Pierce, *Journal of Biomechanical Engineering*, 1987, **109**, 139-147.
53. M. C. Brindise, M. M. Busse and P. P. Vlachos, *Experiments in Fluids*, 2018, **59**, 173.
54. H. E. Bakker, T. H. Besseling, J. E. G. J. Wijnhoven, P. H. Helfferich, A. van Blaaderen and A. Imhof, *Langmuir*, 2017, **33**, 881-890.
55. M. E. Leunissen, C. G. Christova, A.-P. Hynninen, C. P. Royall, A. I. Campbell, A. Imhof, M. Dijkstra, R. van Roij and A. van Blaaderen, *Nature*, 2005, **437**, 235-240.
56. S. J. Lee, H. J. Byeon and K. W. Seo, *Experiments in Fluids*, 2014, **55**, 1-9.
57. P. Torres, M. Balcells, E. Cequier and R. Canela, *Molecules*, 2020, **25**, 2157.
58. A. S. Khair and B. Balu, *Electrophoresis*, 2019, **00**, 1-8.
59. P. G. Saffman, *Journal of Fluid Mechanics*, 1965, **22**, 385-400.
60. F. Feuillebois, *Perturbation problems at low reynolds number*, Centre of Excellence for Advanced Materials and Structures : Institute of Fundamental Technological Research, Warsaw, 2004.
61. R. G. Cox and H. Brenner, *Chemical Engineering Science*, 1968, **23**, 147-173.
62. F. A. Morrison, *Journal of Colloid and Interface Science*, 1970, **34**, 210-214.
63. J. L. Anderson, *Annual Review of Fluid Mechanics*, 1989, **21**, 61-99.
64. M. A. Bevan and D. C. Prieve, *Journal of Chemical Physics*, 2000, **113**.
65. Y. Kazoe and M. Yoda, *Applied Physics Letters*, 2011, **99**.
66. S. Prakash and J. Yeom, *Nanofluidics and microfluidics : Systems and applications*, Elsevier/William Andrew, Amsterdam, 2014.

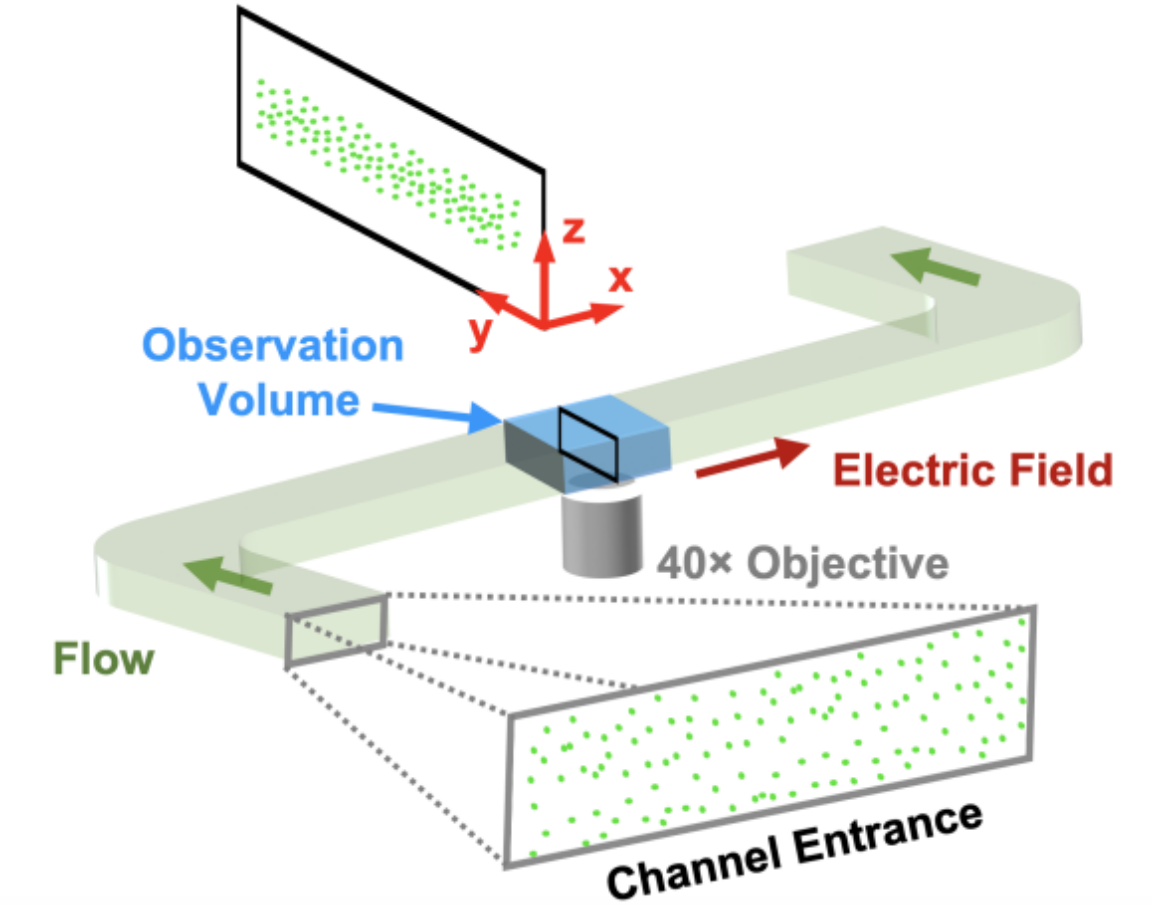

We quantify and investigate the effects of flow parameters on the extent of colloidal particle migration and the corresponding electrophoresis-induced lift force under combined electrokinetic and shear flow.